2D cross-sectional NMR imaging with a simple MRI set-up

Karlo Krakan*
UBC Department of Physics and Astronomy, Vancouver, Canada
(Dated: March 31st, 2017)

Medical imaging requires that any proposed imaging technique must in practice be able to produce useful images at biologically relevant length scales. In this work we find the maximum innate resolution of a simple MRI set-up empirically as $R_{max} = 0.921$mm. Then, two computerized tomography methods, filtered back projection and the simultaneous algebraic reconstruction technique (SART) are used to reconstruct a cross-sectional image of a sample. The small innate resolution of the imaging set-up and the final images demonstrate a proof-of-concept for the viability of MR imaging.

Magnetic resonance imaging (MRI) is a widely used medical imaging modality that is typically used to generate anatomical images of medical patients. The concept from which MRI is based off, nuclear magnetic resonance (NMR), was discovered independently by Felix Bloch [1] and Edward Purcell [2] in the 1940s, for which they shared the 1952 Nobel Prize. The first image of a human with a primitive MRI scanner was performed in the 1970s by Raymond Damadian [3]. Since then, MRI technology and proliferation have increased considerably and MRI has become a very important tool for the medical diagnosis of many illnesses as well as for medical and biological research.

MR imaging is a relatively simple idea, but in practice careful considerations must be taken into account in order to be able to reconstruct the best possible image. The viability of the MR imaging apparatus depends heavily on the strength of the magnetic field gradient which sets the resolution of the imaging apparatus, where stronger gradients mean higher resolutions. To be useful as a medical imaging modality in general, it must be shown that MRI can provide images with a resolution small enough to make out detail on biological length scales.

In this work, a simple MR imaging set-up is used, consisting of a small cylindrical sample in between four pairs of electro-magnetic coils. The innate resolution of this MRI set-up is found empirically and shown to provide a good resolution for medical imaging.

Two computerized tomography methods, filtered back projection and the simultaneous algebraic reconstruction technique (SART) are then used to reconstruct a 2-dimensional cross-sectional image of a sample using the simple MRI set-up mentioned previously. The positive results demonstrate the viability of our simple MRI apparatus. Further, had this been the first experiment of its kind, a positive result would have demonstrated the viability of MR imaging in general and served as a very positive indicator for the viability of more complicated MRI set-ups.

Magnetic resonance imaging is an application of nuclear magnetic resonance (NMR). From quantum mechanics, the proton is known to have a magnetic moment, $\vec{\mu}$ that is quantized,

$$\vec{\mu} = \gamma \vec{J} = \gamma \hbar m_I \hat{I} \tag{1}$$

where $\gamma/2\pi = 42.577\text{MHz}\cdot\text{T}^{-1}$ is the gyromagnetic ratio of the proton, $\vec{J}$ is the quantized angular momentum, $\hbar$ is the reduced Planck's constant, $m_I = -1/2, 1/2$ are the allowed spin projections, and $\hat{I}$ is the direction of the spin. A proton placed in an external static magnetic field $\vec{B} = B_0\hat{z}$ has energy U where

$$U = -\vec{\mu}\cdot\vec{B} = \mu_z B_0 = \gamma\hbar m_I B_0 \tag{2}$$

Since $m_I = -1/2, 1/2$, the proton will have two magnetic energy states in the field $\vec{B} = B_0\hat{z}$. In general, systems like these are known as 2-level systems. The energy separation between these two states is

$$\Delta U = \hbar\omega_0 = \gamma\hbar B_0 \tag{3}$$

$$\omega_0 = \gamma B_0 \tag{4}$$

where equation (3) is the energy seperation and equation (4) is known as the Larmor frequency or resonance frequency, the nomenclature of which shall be explained later. A collection of N protons in the field $\vec{B} = B_0\hat{z}$ will develop a net magnetization according to Boltzmann statistics

$$\vec{M} = M_0\hat{z} = \frac{\gamma\hbar}{2} N \tanh\left(\frac{\gamma\hbar B_0}{2k_B T}\right)\hat{z} \tag{5}$$

where k_B is Boltzmann's constant and T is the temperature of the system. Although there is a net magnetization in the z-direction, quantum mechanics dictates that individual spins actually precess about the direction of the external magnetic field at the Larmor frequency $\omega_0 = \gamma B_0$ but in general each individual spin will have a random phase such that the average net magnetization $\langle M_\perp \rangle$ in the xy-plane is zero.

In practice, in order to be able to measure signal from a collection of spins (henceforth, a sample), it will be necessary to coherently "tip" this net magnetization $\vec{M} = M_0\hat{z}$ into the xy-plane. The resulting dynamics of this tipping process is what allows the signal to be measured.

* karlo@krakan.ca

This is achieved via an additional rotating magnetic field $\vec{B} = B_0\hat{z} + B_1\cos(\omega t)\hat{x}$.

A sample subjected to the static field $\vec{B} = B_0\hat{z}$ at $\infty < t < 0$ and the rotating magnetic field pulse $\vec{B} = B_0\hat{z} + B_1\cos(\omega t)\hat{x}$ at $0 \leq t \leq \tau$ will undergo some complicated dynamics that has the effect of coherently tipping the net magnetization into the xy-plane. To see why this is so, consider changing to a non-inertial coordinate system $x^*y^*z^*$ that is rotating about $\hat{z}$ at frequency ω. In this system, the rotating field becomes the effective field $\vec{B}^*_{eff}$ where

$$\vec{B}^*_{eff} = (B_0 - \frac{\omega}{\gamma})\hat{z}^* + B_1\hat{x}^* \tag{6}$$

Therefore, when $\omega = \gamma B_0$ the effective field points in the $\hat{x}^*$ direction, tipping the magnetization into the xy-plane, hence why equation (4) is also known as the resonance frequency. The time-length τ of the rotating magnetic field pulse can be tuned in order to produce what is known as the $\pi/2$-pulse, a complete coherent tipping of the net magnetization into the xy-plane.

The resulting signal that is produced from a sample following a $\pi/2$-pulse is an exponentially decreasing sinusoid of the form

$$S(t) \propto cos(\omega_0 t)e^{-t/T_2^*} \tag{7}$$

where T_2^* is some characteristic relaxation time of the sample. The resulting signal following a $\pi/2$-pulse is known as the free induction decay (FID) signal.

Now consider two identical samples spatially separated by some distance $\Delta z = z_2 - z_1$ whose spin density $\rho(z)$ can be described by the equation

$$\rho(z) = \rho_0(\delta(z - z_1) + \delta(z - z_2)) \tag{8}$$

where $\delta(x)$ is the ordinary delta function and ρ_0 is the spin density at z_1 and z_2. Following a $\pi/2$-pulse, the resulting signal would look like equation (7) when the sample (8) is subject to the field $\vec{B} = B_0\hat{z}$ as each spin in the sample will be precessing at the same frequency $\omega_0 = \gamma B_0$. In order to be able to image this sample (8), following a $\pi/2$-pulse, the sample is instead subject to a gradient magnetic field of the form

$$\vec{B} = (B_0 + Gz)\hat{z} \tag{9}$$

where G is the gradient in $\mathrm{T{\cdot}m^{-1}}$. Now instead of precessing at the same frequency, each spin in the sample (8) is precessing at a range of resonance frequencies, $\omega_{res}(z)$, given by the spatial position of the spin

$$\omega_{res}(z) = \gamma(B_0 + Gz) \tag{10}$$

Now each point of spin density in the sample (8) is precessing at frequency $\omega_1, \omega_2 = \gamma(B_0 + Gz_1), \gamma(B_0 + Gz_2)$ and so the resulting FID signal will look like

$$S(t) \propto (cos(\omega_1 t) + cos(\omega_2 t))e^{-t/T_2^*} \tag{11}$$

The power spectrum of the signal is defined as

$$P(\omega) = |\hat{S}(\omega)|^2 \tag{12}$$

where

$$\hat{S}(\omega) = \int_{-\infty}^{\infty} e^{-i\omega t}S(t)dt \tag{13}$$

is the Fourier transform of the signal. The power spectrum produced from the sample (8) is therefore

$$P(\omega) = P_0(\delta(\omega - \omega_1) + \delta(\omega - \omega_2)) \tag{14}$$

where P_0 is the energy density at z_1 and z_2. This is a one-to-one mapping of the spin density of the sample (8) along the direction of the gradient into frequency space. In other words, the power spectrum of the signal is a projection of the spin density of the sample along the direction of the gradient.

In practice, the spin density described by (8) will not perfectly produce the power spectrum shown in equation (14), but instead will have some additional Gaussian broadening about ω_1 and ω_2 due to local inhomogeneities in the the external magnetic field as well as random local spin-spin interactions. The broadening is denoted by ΔW. In order to be able to resolve spatially separated points in a sample with separation $\Delta z = z_2 - z_1$, the Guassian broadening of the system must not exceed the difference in resonance frequency $\Delta\omega = \omega_2 - \omega_1$ between the two points. This condition may be stated as

$$\Delta z > \frac{\Delta W}{\gamma G} \tag{15}$$

Therefore, the gradient G must be chosen carefully in order to satisfy this condition. As will be shown later, the signal will be acquired with a digitizing oscilloscope. The digitizing oscilloscope will have some sampling frequency F_s that sets the maximum measurable frequency of the oscilloscope, known as the Nyquist frequency, F_N. This time, in order to be able to measure the signal properly at all, we must have that the difference in resonance frequency $\Delta\omega$ between any two points in the sample is smaller than the Nyquist frequency

$$\Delta z < \frac{2\pi F_N}{\gamma G} \tag{16}$$

When the selection of gradient satisfies both equation (15) and equation (16) then the imaging set-up is viable, where the right hand side of equation (15) defines the resolution of the imaging system. The Guassian broadening ΔW must be found experimentally.

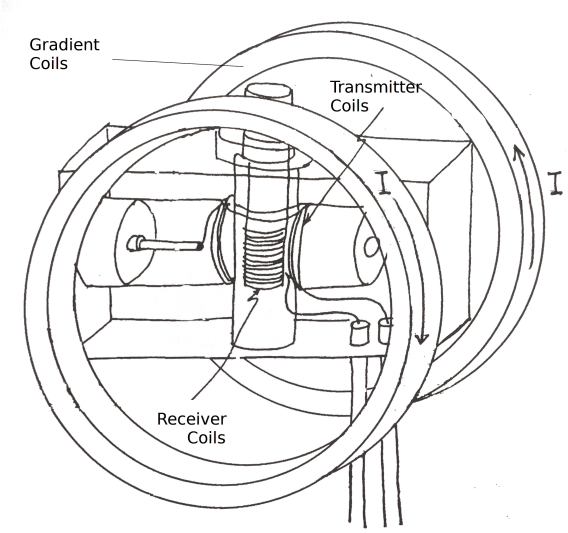

FIG. 1. A pair of Helmholtz coils aligned along the $\hat{z}$ direction produces the main magnetic field B_0. A second set of coils next to the first in anti-Helmholtz configuration and aligned along $\hat{z}$ produces the gradient magnetic field G. A third pair of coils aligned along $\hat{x}$, the transmitter coils, produce the rotating magnetic field needed for the $\pi/2$-pulse. Finally, a single set of coils is wrapped around the sample and aligned along $\hat{y}$. These are the receiver coils used to actually measure the FID signal from the sample.

The imaging set-up used in this work consists of a small cylindrical sample in between four pairs of electromagnetic coils. A diagram of the set-up, with the main Helmholtz coil pair excluded, is shown in Fig. 1.

Fig. 2 shows a block diagram of the signal processing portion of the apparatus.

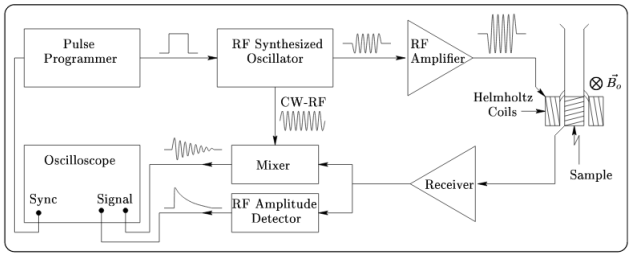

FIG. 2. The pulse programmer, RF synthesized oscillator, and the RF amplifier produce the rotating magnetic field needed for the $\pi/2$ pulse. The RF synthesized oscillator can be tuned so that the rotating magnetic field has frequency $\omega_{rf} = \omega_0$, producing a $\pi/2$ pulse. The signal received from the sample is then fed to a mixer that multiplies the signal from the sample with the signal from the RF synthesized oscillator. The mixer signal is then measured via the oscilloscope. The RF amplitude detector is not integral in this set-up and was only used for tuning and testing purposes

As noted in Fig. 2, the FID signal itself is not measured, rather the output of the mixer is measured. However, the mixer signal has only the (non-trivial) effect of shifting the measured resonance frequencies downwards, $\omega_{measured} = |\omega_{res} - \omega_{rf}|$ where ω_{rf} is the rotating magnetic field frequency set via the RF synthesized oscillator. In this case, the rotating magnetic field must be tuned slightly off-resonance, ie. $\omega_{rf} > \omega_0$, so that the measured frequencies are non-zero. Although this does not correspond to a true $\pi/2$-pulse, the difference is negligible, at least for the purposes of this work. The signal from the mixer is of the same form as equation (11). For the sample described by equation (8), the mixer signal is

$$S(t) \propto [cos(|\omega_1 - \omega_{rf}|t) + cos(|\omega_2 - \omega_{rf}|t)]e^{-t/T_2^*} \quad (17)$$

The Gaussian broadening ΔW of the two signals is the same. This signal is measured via the oscilloscope.

As stated previously, in order for this set-up to be viable for imaging, the criteria (15) and (16) must be satisfied. The gradient coils described in Fig. 1 produce the following gradient

$$G = N\frac{\mu_0 I R^2}{(a^2 + 4R^2)^{5/2}} \quad (18)$$

where $N = 100$ is the number of turns, μ_0 is the vacuum permeability, I is the current, $a = 0.057$m is the separation of the coils, and $R = 0.0925$m is the radius of the coils. At current $I = 9$A, these coils produce a gradient $G = 0.098\text{T}\cdot\text{m}^{-1}$. The maximum extent of the cylindrical sample is $\Delta z = 0.0077$m. The Nyquist frequency of the oscilloscope is $F_N = 100$Mhz. With these numbers, the selected gradient at $I = 9$A satisfies condition (16).

To determine the resolution of the imaging system and to check whether or not the system satisfies condition (15), the Guassian broadening ΔW must be measured.

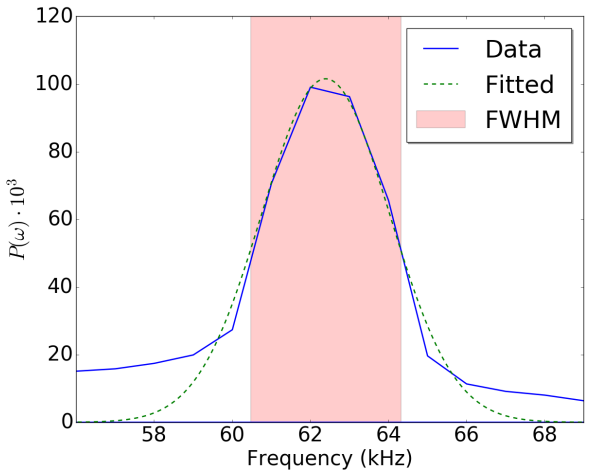

FIG. 3. The Gaussian broadening of the imaging system ΔW. The data is shown in the blue line, while the green line is a fitted Gaussian. ΔW is the full-width-half-max of the power spectrum, shown in light red. The Gaussian broadening is calculated as $\Delta W = 3.858$kHz for the fitted spectrum with the gradient $G = 0.098\text{T}\cdot\text{m}^{-1}$.

The Gaussian broadening is defined as the full-width-half-max (FWHM) of the power spectrum of the real FID signal produced by a point source subject to the gradient field. In our case, a point source is approximated via the sample and therefore the calculated broadening actually corresponds to a maximum resolution. The FWHM is found in Fig. 3, showing that the system is viable. The maximum resolution with gradient $G = 0.098\text{T}\cdot\text{m}^{-1}$ is

$$R_{max} = 0.921\,\text{mm} \tag{19}$$

Which is viable since $0.921\text{mm} < \Delta z = 7.7\text{mm}$, satisfying condition (15).

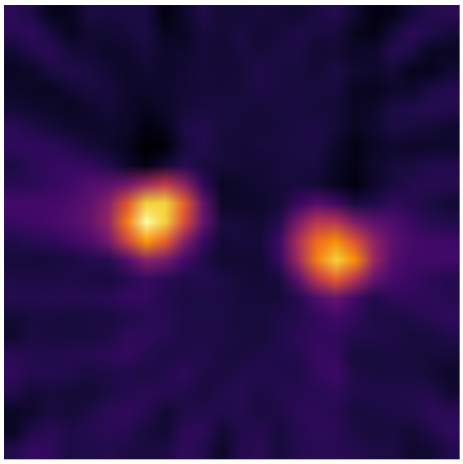

FIG. 4. An image of a sample reconstructed with the filtered back projection. The sample was turned through 0-180° at 15° increments and a projection of the sample measured at each angle. The data was taken with a gradient of $G = 0.098\text{T}\cdot\text{m}^{-1}$.

The object to be imaged is a small cylindrical sample with diameter $\Delta z = 7.7\text{mm}$ made out of a material which does not interact with the magnetic fields but which has two small holes drilled side by side filled containing a fluid (likely water or glycerin) which does interact with the magnetic field as described in this work. The spin density of this sample is similar to the form in equation (8). To image the sample, we use the above method to obtain projections of the spin density of the sample along the direction of the gradient. The sample is turned through 0-180° in order to measure the spin density along many projections angles. The resulting data can be reconstructed with filtered back projection (FBP) or the simultaneous algebraic reconstruction technique (SART). Fig. 4 and 5 show the results of each reconstruction. Each measurement of the power spectrum at each angle is averaged via the oscilloscope 512 times in order to reduce statistical uncertainty.

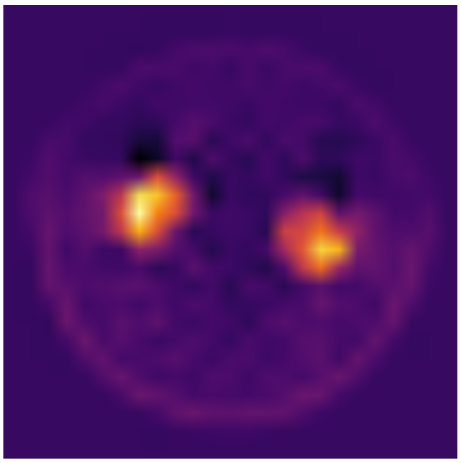

FIG. 5. An image of a sample reconstructed with the simultaneous algebraic reconstruction technique with 10 iteration. The sample was turned through 0-180° at 15° increments and a projection of the sample measured at each angle. The data was taken with a gradient of $G = 0.098\text{T}\cdot\text{m}^{-1}$

A faint star-like artifact can be seen in Fig. 4, indicating that more projection angles should have been taken. However, our set-up makes it quite difficult to turn the sample in any smaller increments and so this is not done. The SART reconstruction in Fig. 5 does not show these artifacts.

As shown in the figures, the imaging system has worked to provide clear cross-sectional images of the sample after the system was shown to be viable to produce images. Had this been the first work of its kind, this positive result in this work would have been an indication for the viability of more complicated MRI set-ups to be used for medical imaging. Although the sample used in this work was not suitable to this end, further work can be done to test contrasting methods such as T_1 and T_2 contrasting which can greatly affect the final images.

[1] F. Bloch, Phys. Rev., **70**, 460 (1946).
[2] E. M. Purcell, H. C. Torrey, R. V. Pound, Phys. Rev., **69**, 37 (1946).
[3] R. Damadian, M. Goldsmith, L. Minkoff, Physiol. Chem. Phys., **9**:97-100, 108 (1977).